Marginal integrity in minimally invasive molar resin composite restorations: Impact of polymerization shrinkage

journal of the mechanical behavior of biomedical materials 155 (2024) 106554

Contents lists available at ScienceDirect

Journal of the Mechanical Behavior of Biomedical Materials

journal homepage: www.elsevier.com/locate/jmbbm

Marginal integrity in minimally invasive molar resin composite restorations: Impact of polymerization shrinkage

Dominique Weimann [a], Claudia Fleck [a,**], Hajar Razi [b,c,*]

[a] Materials Science and Engineering, Technische Universität Berlin, Berlin, Germany
[b] ETH Zurich, Zurich, Switzerland
[c] WoodTec Group, Cellulose & Wood Materials Laboratory, Empa, Dübendorf, Switzerland

ARTICLE INFO

Keywords:
Selective caries removal
Tooth-restoration marginal integrity
Polymerization shrinkage
Minimally invasive dentistry
Nonlinear finite element modeling
Failure/crack modeling

ABSTRACT

Objectives: This study utilized non-linear finite element (FE) models to explore polymerization shrinkage and its impact on marginal integrity in molars following both selective caries removal (SCR) and conventional treatment. Specifically, we performed 2D in silico simulations to study residual stresses post-resin polymerization shrinkage and their influence on the marginal integrity of various restoration types.

Methods: Initially, FE models were developed based on a cohesive zone framework to simulate crack propagation along the bonded interfaces between restoration and tooth structure in SCR-treated molars with class I and class II restorations. The modeled resin composite restorations first underwent polymerization shrinkage and were then subjected to various occlusal loading conditions. Stress magnitudes and distributions were identified to evaluate the margin integrity and predict the mechanism and location of interfacial failure.

Results and discussion: The FE models computed polymerization shrinkage stresses of less than 1 MPa, exerting a minor influence on the composite/tooth interface. Occlusal loading, however, significantly impacted the load-bearing capacity of the composite/tooth (c/t) interface, potentially jeopardizing the restoration integrity. Especially under bi-axial occlusal loading, interfacial debonding occurred in the vertical cavity walls of the class I restorations, increasing the risk of failure. Notably, SCR-treated teeth exhibited better margin integrity than restored teeth after complete caries removal (NCR).

These findings provide valuable insights into the mechanical behavior of SCR-treated teeth under different loading conditions and highlight the importance of considering the load scenarios that may lead to failure at the c/t interface. By investigating the factors influencing crack initiation and delamination, this novel research contributes to the optimization of restorative treatments and aids in the design of more resilient dental restorations.

1. Introduction

Selective caries removal (SCR) represents a paradigm shift in dentistry, offering a minimally invasive approach to managing deep cavitated carious lesions while conserving demineralized and non-carious tooth tissue (Lim et al., 2023; Widbiller et al., 2022).

Unlike conventional methods, SCR leverages the intrinsic healing potential of dentin affected by caries, enabling the mechanical restoration of weakened teeth (Alves et al., 2010; Jardim et al., 2020). This innovative technique involves meticulous removal of carious tissue from the cavitated periphery while retaining demineralized dentin near the pulpal floor, thus preserving the weakened dentin's structural integrity and pulp vitality (Schwendicke et al., 2019; Widbiller et al., 2022). SCR has demonstrated remarkable efficacy in both primary and permanent teeth across various clinical studies, highlighting its versatility and reliability in modern restorative dentistry (Franzon et al., 2015; Gözetici-Çil et al., 2023; Jardim et al., 2020; Maltz et al., 2013).

However, SCR strategies require specific consideration in the selection of restorative materials and adhesives regarding the bonding and restoration integrity. Resin-based composites are often used due to their mechanical and aesthetic properties (Tjäderhane and Tezvergil-Mutluay, 2019). Despite their advantages, resin composites

* Corresponding author. ETH Zurich, Zurich, Switzerland.
** Corresponding author.
E-mail addresses: claudia.fleck@tu-berlin.de (C. Fleck), harazi@ethz.ch (H. Razi).

https://doi.org/10.1016/j.jmbbm.2024.106554
Received 29 January 2024; Received in revised form 11 April 2024; Accepted 12 April 2024
Available online 18 April 2024

present inherent challenges, including the potential for unstable bonding with dentin due to inadequate infiltration of the adhesive system into the demineralized dentin matrix (Betancourt et al., 2019). The complex nature of dentin, characterized by dentin tubules embedded in a collagen matrix, poses additional challenges in achieving a reliable bond with restorative materials. The effectiveness and strength of the bond between the composite material and dentin play a crucial role in distributing and managing stresses within the restoration. A robust bond ensures efficient stress transfer during polymerization shrinkage, reducing the risk of debonding or microleakage at the restoration interface (Betancourt et al., 2019; Di Lauro et al., 2023).

Moreover, the polymerization process of resin composites induces residual shrinkage stresses compromising the long-term stability of the restoration. The volumetric shrinkage, induced by solidification of the composite, develops during pre-gel and post-gel phases. Throughout the pre-gel phase, the resin is viscous and flows, relieving residual stresses resulting in negligible shrinkage stresses (Davidson and Feilzer, 1997; Lins et al., 2019a). During the transition from the pre-gel to the post-gel phase, the resin matrix of composites changes from a viscous paste to an elastoplastic solid with increased stiffness (Cakir et al., 2007; Sakaguchi et al., 2004). This transition fosters the formation of a compact polymer network, leading to volumetric shrinkage and a denser structure, thus a decreased stress relaxation capacity of the material (Soares et al., 2013; Versluis et al., 2004; Wang et al., 2011).

In the context of dental restoration, the constrained polymerization of composite resin results in anisotropic shrinkage, leading to clinically significant residual stresses within the restoration and at the composite-tooth interface (Braga et al., 2006; Mantri and Mantri, 2013; Soares et al., 2017). These stresses can compromise the adhesive bond strength, leading to clinical issues such as marginal debonding, heightening the risk of postoperative pain and recurrent caries (Elgezawi et al., 2022; Kleverlaan and Feilzer, 2005; Li et al., 2014).

Despite ongoing efforts to characterize polymerization shrinkage, literature values remain contentious. Total volumetric shrinkage in resin-based composites ranges from 1.5% to 6% (Boaro et al., 2010; Hirata et al., 2015; Kleverlaan and Feilzer, 2005). Post-gel shrinkage, a key contributor to residual stresses, is typically measured between 0.075% and 0.96% (Bicalho et al., 2014; Correia et al., 2018; Soares et al., 2013). Various techniques, including strain gauge analysis and uni-axial or cantilever-based instruments, have been employed to assess residual shrinkage stresses (Rajan et al., 2019; Chiang et al., 2011). Likewise, non-invasive computational methods such as finite element analysis (FEA) are utilized for assessing shrinkage stresses (Chen et al., 2014; Soares et al., 2017). FEA employs a thermal analogy to model polymerization shrinkage, facilitating examination of residual stresses in restored teeth:

$$\Delta V/V = 3 * \alpha * \Delta T$$

In this equation, ΔV, V, α, and ΔT are the change in volume, original volume, the coefficient of linear thermal expansion (CTE), and temperature change, respectively. The term ΔV/V represents the isotropic volumetric strain (i.e., volumetric shrinkage), and to derive the linear shrinkage value (i.e., linear strain), ΔV/V must be divided by three (Soares et al., 2013).

In the early '90s, Hickmann and Jacobsen employed a thermal approach to simulate shrinkage in a restored FE tooth model (Hickmann and Jacobsen, 1991). They used a linear shrinkage value of 0.00333 as CTE to achieve a desired 1% volumetric shrinkage, assuming a virtual temperature change of one degree (Hickmann and Jacobsen, 1991; Soares et al., 2013). Recent FE studies still utilize these data (Ausiello et al., 2017; Bicalho et al., 2014; Laughlin et al., 2002), while others prefer experimental "post-gel" shrinkage values (Bicalho et al., 2014; Correia et al., 2018; Da Silva Pereira et al., 2020; Soares et al., 2013). Regardless of total or post-gel CTE, shrinkage stresses, predicted by FE simulations, are often tenfold higher (Dejak and Młotkowski, 2015; Soares et al., 2017) than experimental measurements, highlighting the need for further understanding of the underlying modeling assumptions (Boaro et al., 2010; El-Damanhoury and Platt, 2014; Fronza et al., 2015; Ilie and Hickel, 2011; Keβler et al., 2019; Kim et al., 2015) (Fig. S1).

In our research, we aim to address controversies in shrinkage stress reports by evaluating residual stresses and the resultant restoration structural integrity post-SCR treatment. Here, we focus on class I and class II cavities while utilizing FEA. Specifically, we analyze stress distribution and interfacial crack propagation in SCR-restored teeth through three clinically relevant stages: immediately after post-gel polymerization shrinkage, post-polymerization shrinkage under various occlusal loads, and post-remineralization of demineralized residual lesions. Additionally, we compare our findings to conventional treatment. We test the hypothesis that the SCR-treated tooth will perform superior in marginal integrity than the complete carious removal. We propose that the remineralization of the residual lesions influences the tooth biomechanical performance, and it enhances the longevity of the restoration.

2. Material and methods

2.1. Theoretical background - cohesive zone modeling

The formulation of cohesive zones is a popular computational tool to predict debonding effects and cracks in heterogeneous materials (i.e., bi-layers). Cohesive zone modeling emulates the traction σ - separation δ relation between two bonded surfaces and includes damage initiation and evolution conditions for progressive damage (Haddad and Sepehrnoori, 2015). The σ - δ relation specifies three bond conditions at the interface: intact bond, debonding, and detached conditions (Harper and Hallett, 2010) as illustrated in Fig. 1a.

The bond between the surfaces remains linear elastic until the bond strength T limit is exceeded (Ikramullah et al., 2020). As a result of exceeding T, the adhesion at the interface is corrupted, which induces the debonding process. The bond is completely detached when no stress can be transmitted any longer. Integrating the traction-separation law up to failure δ_{fail} (detached bond) yields the area under the σ - δ curve. This area corresponds to the dissipated work during bond separation, named the critical energy release rate Gc (Gilabert et al., 2015; Paneda, 2018).

The general stress state at the interface of bonded surfaces can be partitioned into three components: the tensile stress (σ_I) and two shear stresses (in-plane: σ_{II} and out-of-plane: σ_{III}). They correspond to the three key crack loading modes (Fig. 1b). Fig. 1c shows the traction-separation relation on the σ - δ_{normal} plane under mode I (blue triangle in Fig. 1c), and on the σ - δ_{shear} plane under mode II (red triangle in Fig. 1c). The shear components are assumed to be the same (i.e., $\sigma_{II} = \sigma_{III}$) and represented as mode II (red triangle in Fig. 1c). Under mixed mode loading, the maximum traction stress and the critical separation are used to determine damage initiation. This approach considers a quadratic relation between the stresses recorded in all three loading directions (quadratic failure criterion) (Bedon et al., 2018; Harper and Hallett, 2010). The critical energy release rate G_C is used to govern the damage evolution of the bond. G_C corresponds to a mixed loading configuration where the influence of normal and shear modes is supposed to be superimposed in the adhesive (Fig. 1c) (Jousset and Rachik, 2014). It is described by Benzeggagh and Kenane's (BK) damage evolution criterion, which is useful when the critical fracture energies during deformation purely along the first and the second shear directions are the same: i.e., $G_{IIC} = G_{IIIC}$ (Abaqus User Manual). The BK damage evolution criterion is expressed as:

$$G_C = G_{IIC} + (G_{IIC} - G_{IC}) \left\{ \frac{G_{IIC}}{G_{IIIC}} \right\}^{\eta}$$

where G_{IC}, G_{IIC}, G_{IIIC} are respectively critical fracture energies during

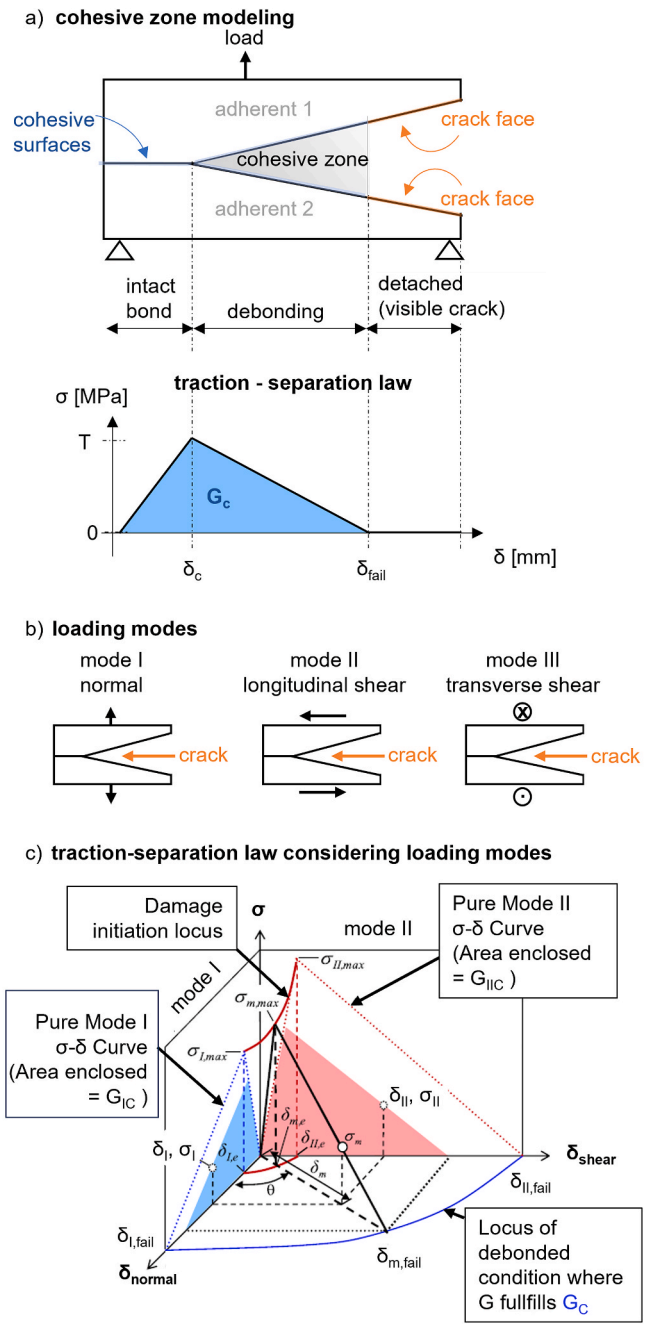

Fig. 1. Cohesive zone modeling (CZM) with damage initiation and crack propagation. a) The cohesive surfaces represent an initially bonded interface between two adherents under normal load that causes tensile stresses around the interface. The damage initiation marks the beginning of the cohesive fracture zone (debonding) and occurs perpendicularly to the applied load at maximum tensile stress. The increasing separation of the adherents to each other results in decreasing fracture energy ending up with a crack tip. b) Basic modes of crack extension which can occur at the interface of bonded surfaces. c) Traction-separation law for mixed-mode I/II loading. Figure adapted after Harper et al. with permission (Harper and Hallett, 2010).

deformation along the normal and shear directions. The factor η is a material parameter (Haddad and Sepehrnoori, 2015). For isotropic material behavior, the critical fracture energies in all modes are the same (i.e., $G_{IC} = G_{IIC} = G_{IIIC}$) which simplifies the equation to:

$$G_C = G_{IC}$$

The quadratic failure criterion and the BK damage evolution criterion have been successfully used to predict mixed-mode damage initiation in (Shao et al., 2022).

2.2. Finite element modeling

2.2.1. Generation of 2D FE tooth models based on a 3D model

The 3D model included the healthy human third molar captured through micro-computed tomography (SkyScan 1172 μCT, Bruker, Billerica, USA).The tooth sample was obtained under an ethics protocol approved by the ethics committee of the Charité – Universitätsmedizin Berlin EA4/102/14. As summarized in our previous work (Weimann et al., 2021), the μCT data were cropped, down-sampled, and then visualized as grey-scale patterns. Enamel, dentin, and pulp could be clearly differentiated based on the grey-scale spectrum and were segmented into three volumes (Fig. 2a). We sliced the 3D model in an apical direction to obtain a mesiodistal section in 2D (HYPERMESH, v.20, Altair Engineering Inc. Troy, Michigan, USA) (Fig. 2b and c). The 2D section was then imported into ABAQUS/CAE 2021 software (Dassault Systémes Simulia, Johnston, RI, USA) to build a representative 2D tooth model with the original contour. Based on the 2D section, six 2D FE models of restored teeth with different modifications were designed. Four of the FE models represented restored teeth after selective caries removal (SCR) and two of them after nonselective caries removal (NCR). We introduced either occlusal class I restoration or mesial class II restoration. In SCR models, the cavity of class I had an intercuspal width of 3.4 mm and a depth of approx. 3 mm in apical direction, while the class II cavity had an axial wall of 4.5 mm and a gingival floor of 2 mm in length. Both cavities had rounded angles (i.e., fillet at the corners) to avoid arbitrarily large stress concentrations. We further assumed two different recovery stages in SCR-treated teeth. The first stage described the restored teeth with carious lesions shortly after SCR treatment, and the second one considered SCR-treated teeth with remineralized lesions that had undergone a recovery process (remineralization). For the first stage, the carious lesions were modeled as truncated cones as described previously (Weimann et al., 2021). The lesion extent varied between 3 and 1 mm, while its depth was kept constant with a value of 1 mm. To simulate the recovery process of the lesion, we modified the SCR models with carious lesions by replacing the lesions with healthy dentin.

In NCR models, carious lesions were assumed to be fully removed. As a result of the caries removal, the class I and class II cavities were extended by 0.25 mm towards the pulpal floor and thus larger than those in SCR teeth.

The following summarizes all six FE models, each with the given modifications (Fig. 2d and e):

I) SCR-I, carious: SCR-treated molars with occlusal class I restoration placed above a carious lesion. The class I restoration was centered on the enamel-dentin volume.
II) SCR-I, remineralized: SCR-treated molars with occlusal class I restoration placed above a carious lesion. The class I restoration was centered on the enamel-dentin volume.
III) NCR-I: NCR-treated molar with occlusal class I restoration
IV) SCR-II, carious: SCR-treated molars with proximal class II restoration on the mesial side neighboring the carious lesion.
V) SCR-II, remineralized: SCR-treated molars with proximal class II restoration on the mesial side neighboring the carious lesion
VI) NCR-II: NCR-treated molar with proximal class II restoration.

The feasibility and accuracy of the 2D models were evaluated and considered as sufficiently precise. Under identical boundary conditions, the 2D models could reproduce similar results as those in 3D tooth models with the same class configuration presented in our previous study (Fig. S2).

The mesh generation details of all models are included in section 2.2.2.

One 3D image of a healthy human third molar was captured through

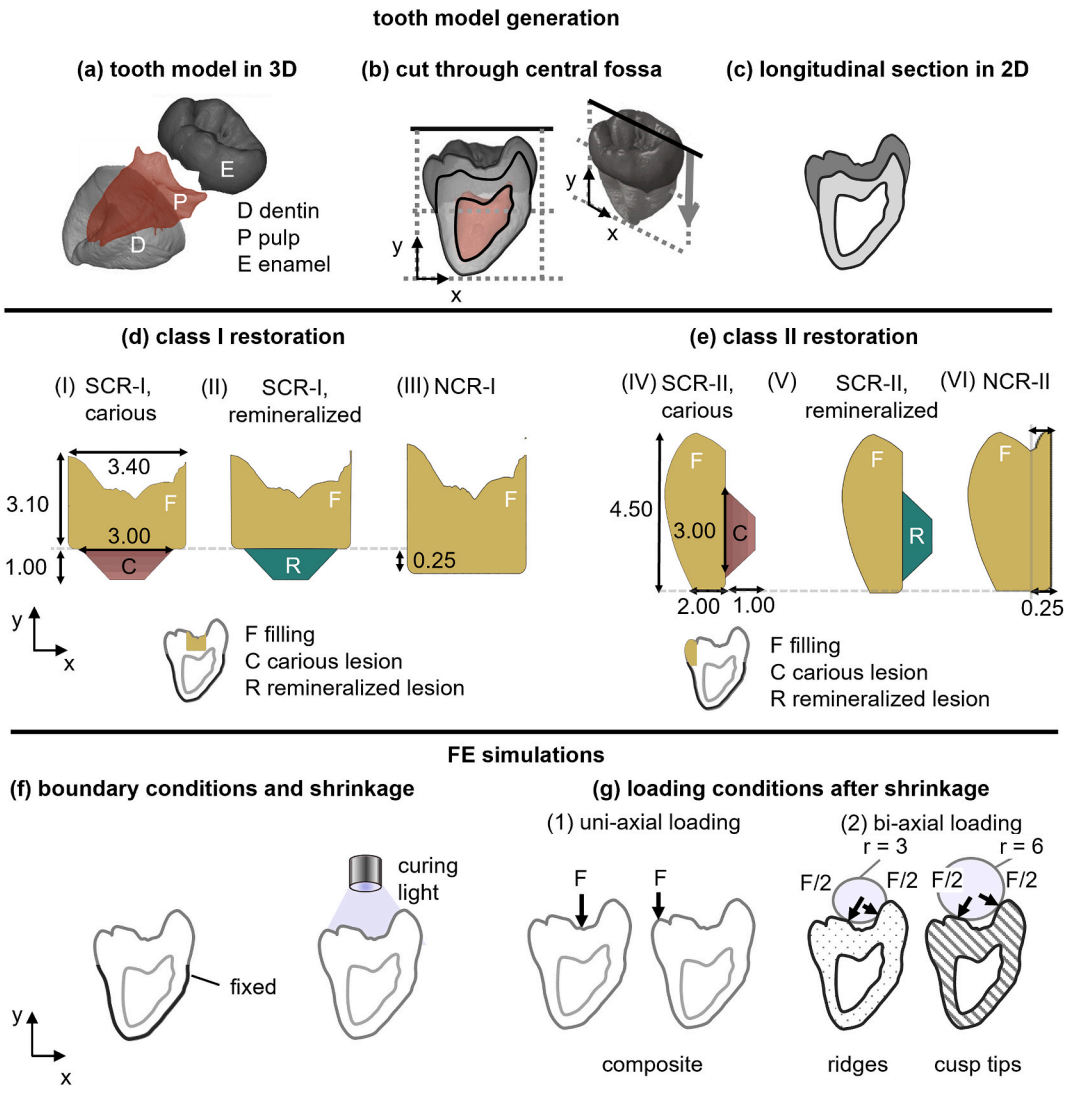

Fig. 2. Overview of the tooth model generation and finite element (FE) simulations.

micro-computed tomography (a) and sectioned through the central groove along the longitudinal axis (b). The resultant contour of the section was used to construct a FE tooth model in 2D (c). Restorations were placed either occlusally as class I (d) or proximally as class II (e). The sizes are given in mm. The exterior root was fixed, and polymerization shrinkage was simulated parallel to the long axis of the teeth in class I and class II restoration (f). The occlusal surface was then loaded (g). Under uni-axial loading, the composite is vertically loaded with F = 100 N. Under bi-axial loading, the point loads (F/2 = 50 N) were applied on the mesial and distal ridge. The distance of both point loads corresponds to contact areas of an imaginary ball indenter with radii of 3 mm and 6 mm lying on the occlusal surface. The radius r is marked and given in mm.

2.2.2. Meshing and boundary conditions

All 2D models were meshed with approx. 15×10^4 plane-strain elements (CPE4I) with manual control to ensure proper refinement at the areas of interest (e.g., dental walls of the restoration) and with focus on homogeneity, congruence, and adequate (e.g., one to one) connectivity between composite and tooth structures (Fig. S3). The interface between composite and tooth tissue was modeled as an adhesive contact by defining a cohesive zone in Abaqus/CAE 2021. We used cohesive elements with quadratic failure criterion and BK criterion to predict debonding at the composite/tooth interface. All other material interfaces (e.g., enamel-dentin and dentin-carious lesion) were assumed to be fully bonded i.e., meshed surface points where dentin and enamel connect deform the same for both tissues. To prevent translatory movement, the exterior root (zero-displacements in both horizontal and vertical directions) was fixed in all models (Fig. 2f).

2.2.3. Material properties

Tooth models included four material entities: enamel, dentin, resin composite (filling material), and carious lesion. Each entity was assumed to be linear-elastic, isotropic, and homogenous. To ensure comparability, we chose the same material data as assumed in our previous study (Weimann et al., 2021). The elastic moduli and Poisson's ratios are listed in Table 1.

Since the pulp is much softer than the other tissues or materials, it was excluded from the FEA model in order to simplify the analysis and reduce the computation cost. For the restoration, a bulk-fill resin composite was chosen. The time dependent behavior of the elastic modulus of the resin composite was not taken into account, as its effect on the margin integrity has been reported to be minimal during polymerization shrinkage (Chen et al., 2014; Chuang et al., 2011). The elastic modulus of the composite was therefore considered to be that of the cured composite. While the material properties of healthy tooth tissues and dental composite are well investigated, less certainty exists regarding the structural heterogeneity and properties of the carious lesions (Pugach

Table 1
Material properties used in the finite element models.

tooth tissue	Young's modulus E [MPa]	Poisson's ratio ν [-]	Coefficient of thermal expansion α [10^{-6}/°C]	Tensile bond strength T [MPa]	Critical energy release rate G_c [MPa*mm]
enamel	100 000	0.30			
dentin	19 800	0.31			
filling	15 000	0.30	21.97		
residual lesion:					
layer L_1	1600	0.35			
layer L_2	6150	0.34			
layer L_3	10700	0.33			
layer L_4	15250	0.32			
bond between tooth and composite	–	–	–	8.56	0.02

et al., 2009). We, therefore, modeled the residual lesion as a four-layered material system with different material properties in each layer (Table 1) as previously explained in detail (Weimann et al., 2021).

2.2.4. Contact properties

The interaction between the external surface of the filling and the internal surface of the tooth cavity relies on a surface-based cohesive behavior governed by bilinear traction–separation law (ABAQUS/CAE, 2021). This assumption is intended for cases where the adhesive is too thin, as its physical thickness could be accurately defined as its physical thickness (Diehl, 2008). The contact properties were taken from fracture tests of restored teeth that were numerically verified and thus suitable to describe the bond between tooth and resin composite (Li et al., 2011). The properties are listed in Table 1. As we assumed isotropic behavior in the entire model, we considered the bond strength T and the critical energy release rate G_C to be the same in all directions, respectively.

2.2.5. Polymerization shrinkage

For modeling polymerization shrinkage, the thermal analogy was used. This approach to the modeling of polymerization shrinkage has been used in previous studies (Boaro et al., 2010; Chen et al., 2014; Da Silva Pereira et al., 2020; Soares et al., 2013).The resultant shrinkage stresses σ are therefore governed by the following equation:

$$\sigma = E * \alpha * \Delta T$$

where E and α are Young's modulus and the coefficient of linear thermal expansion (CTE) of the composite, respectively. The CTE of bulk fill resin composites has been reported to span 10.3–37.1 (10^{-6}/°C) (Nascimento et al., 2019). Here, a resin material made of bis-GMA was taken from literature showing a thermal coefficient α of 21.97 (10^{-6}/°C) (Alnazzawi and Watts, 2012). The temperature change ΔT was assumed to be a drop of one degree.

2.2.6. FE simulations

All models were subjected to the following loading scenarios: (1) isotropic polymerization shrinkage by curing the composite parallel to the long axis of the teeth, and (2) polymerization shrinkage and masticatory forces acting on the occlusal portion (Fig. 2f and g). To represent a variety of masticatory conditions, four occlusal loading conditions were performed across the crown surface. The force F of 100 N was simulated as point load which was applied on the composite in the vertical direction (uni-axial loading).

Under bi-axial loading, in contrast, the force of 100 N was split in half (F/2) and applied obliquely at the ridges/cusp tips with an angle of 45° to the long axis of the tooth causing normal and shear force components. The positions of load introduction were a priori identified as contact points by placing perfect spheres with radii of 3 and 6 mm on the crown surface and examining the contact areas (Fig. 2i). The total force amount was supposed to be 100 N for the following reasons:

i) to keep comparability to other FEA studies (Robinson et al., 2019),
ii) as 100 N is a realistic biting force that has been determined during chewing (Lundgren and Laurell, 1986) and
iii) it is often assumed in several experimental studies (Lins et al., 2019b).

FEM calculations were conducted by the commercial solver ABAQUS/STANDARD 2021 (Dassault Systémes Simulia, Johnston, RI, USA). Mesh convergence testing was successfully performed (Fig. S5).

3. Results

High stress levels may lead to loss of adhesion between the composite restoration and the tooth structure. This loss of adhesion can compromise the structural integrity of the restoration and eventually lead to the fracture of the restored tooth (Peutzfeldt, 1997). By employing the von Mises criterion, we were able to qualitatively evaluate the mechanical performance of materials. Therefore, in sections 3.1 and 3.2, von Mises criterion was utilized in order to assess potential mechanical failure at the composite-tooth (c/t) interface under two specific conditions (Moga et al., 2023): post shrinkage, and post shrinkage and subjected to external load. In section 3.3, the initiation of crack and subsequent delamination along the c/t interface in SCR-treated teeth are reported based on fracture mechanics predictions in the FE models.

In the following sections, the stresses reported were measured at different areas inside the composite. The stresses close to the c/t interface and those in the very center of the composite bulk are called *interfacial* and *internal* stresses, respectively.

3.1. Residual shrinkage stresses after polymerization shrinkage

Von Mises stresses induced after polymerization shrinkage are shown in Fig. 3 in SCR-treated molars with class I (top) and class II (bottom) restoration. For class I and class II restoration, the models predicted double peaked stress distribution at the c/t interface, with maximum von Mises stress levels of 0.75 MPa in class I and 0.80 MPa in class II. The maximum stresses were detected along the dental walls in proximity to the crown surface and were nearly 50% larger than those observed inside the composite and those at the pulpal c/t interface.

Von Mises stresses were computed along paths p_I and p_{II} inside the composite of SCR-treated teeth with class I (top) and class II (bottom) restoration. The paths were set at the composite/tooth (c/t) interface (red arrow) and inside the composite along the exterior and interior of the restorative material (brown and blue arrow). The length of each path was normalized to facilitate the comparison between the different stress profiles. The orange arrows in the diagram highlight the maximum von Mises stresses along the c/t interface. The interfacial mean stresses along the c/t interface $\bar{x}_{c/t}$ were calculated. For sake of clarity, the carious lesion neighboring the composite is not shown.

We then examined the influence of polymerization shrinkage in

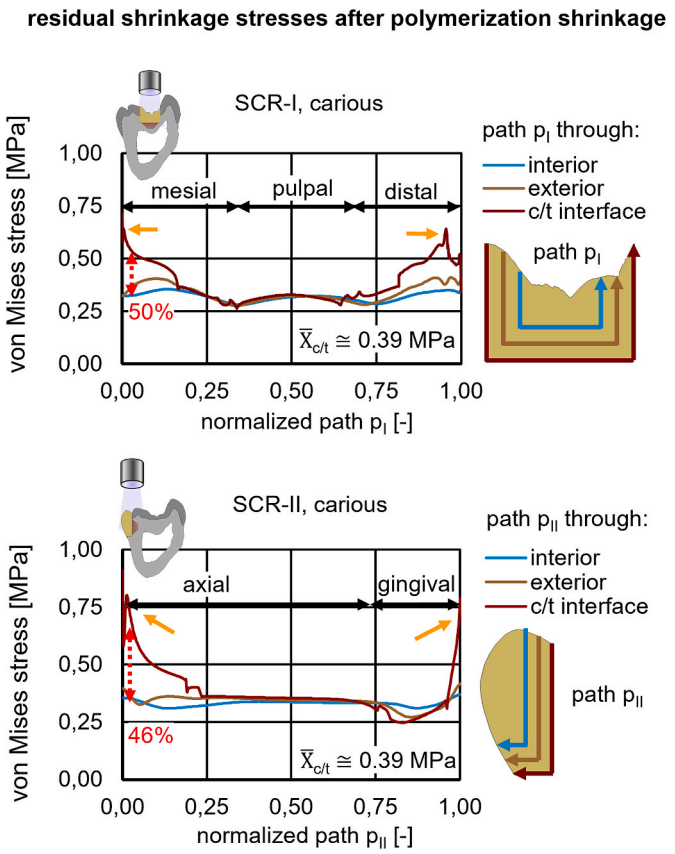

Fig. 3. Influence of polymerization shrinkage on the mechanical integrity of the resin composite adhesively bonded to tooth tissue.

molars treated after SCR vs. NCR (i.e., nonselective caries removal). Our simulations showed that SCR and NCR treated molars exhibited similar stress distributions at the c/t interface after the simulated shrinkage (Fig. S4). The maximum stresses in SCR were in a similar range (−4%) as those observed in NCR teeth.

3.2. Stress response under various occlusal loading conditions

In this section, all models presented underwent polymerization shrinkage and were then subjected to various occlusal loading scenarios. The stress distribution and magnitude along the c/t interface in all models are presented in Figs. 4 and 5. Assuming a bond strength of 8.56 MPa (Li et al., 2011), regions of the c/t interface prone to failure are shown in the figures.

We simulated a series of bi- and uni-axial loading conditions at the occlusal portion of the tooth with class I **restoration** following SCR or NCR treatment and post polymerization shrinkage (Fig. 4). In SCR-treated teeth, the bi-axial loading at the tooth ridges (Fig. 4, left) induced the largest von Mises stresses (of up to 60 MPa) at the mesial c/t interface compared to the other loading cases. Thus, the stress values at the mesial c/t interface in SCR-treated tooth under bi-axial load at ridges largely exceeded the bond strength of the tooth-restoration complex. The area at the mesial c/t interface was highly prone to failure. SCR teeth with loaded cusps (cusp tips loading) showed the lowest stresses, amounting to less than 5 MPa along the entire c/t interface (Fig. 4a). Under uni-axial loading, a concentrated force of 100 N induced maximum von Mises stresses of up to 13 MPa in SCR-treated tooth, resulting in regions of mesial, pulpal, and distal c/t interface prone to failure. The maximum stresses susceptible to failure were located in proximity of the pulpal floor, particularly at the interface between the composite and the residual lesion (Fig. 4b). We then analyzed SCR-treated tooth with remineralized lesions and caries-free teeth after NCR. In both models, the restorations were subjected to uni-axial loading, assumed as the most susceptible loading scenario with risk for fracture. Apart from the distal c/t interface, SCR-I with remineralized lesion and NCR-I (caries-free) did not show pronounced stresses along the c/t interface, especially high stresses in proximity of the pulpal floor as those observed in SCR-treated teeth were absent (Fig. 4b).

In **class II restoration** after SCR treatment, bi-axial loading (loaded ridges and cusp tips) induced no pronounced stress values along the axial wall (Fig. 5a). Under both bi-axial loading conditions, the von Mises stress level remained below the interfacial bond strength. In contrast, the uni-axial loading of the restoration in SCR-treated teeth

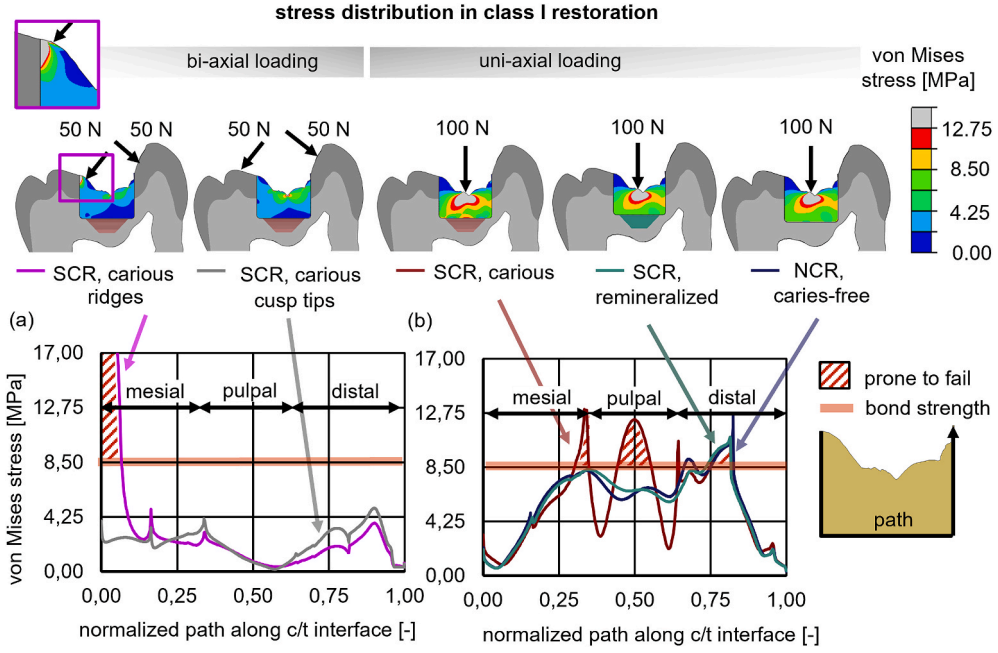

Fig. 4. Stress contour plots of the composite under bi-axial (left) and uni-axial loading (right). Von Mises stresses were plotted against path p running along the composite-tooth (c/t) interface.

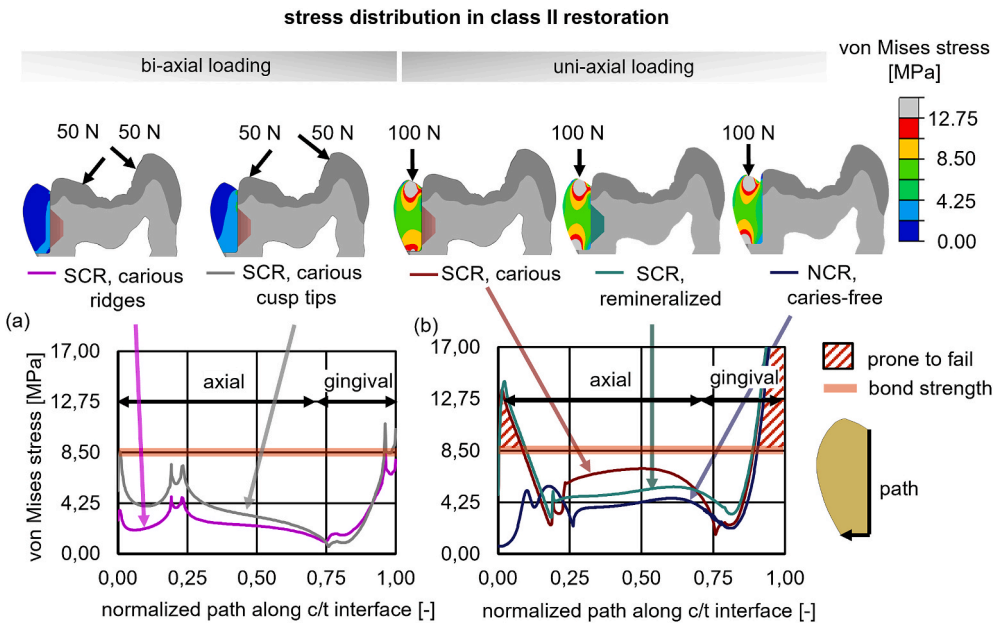

Fig. 5. Contour plots of von Mises stress in SCR treated tooth with class II restoration under loaded ridges and cusp tips with 50 N each (bi-axial loading, left) and under a load of 100 N applied on the composite (uni-axial loading, middle). Moreover, von Mises stresses were shown for an SCR treated tooth with remineralized lesion and in a caries-free tooth after NCR under uni-axial loading. The value of the bond strength between composite and tooth is highlighted as a horizontal line. (a) Von Mises stress distribution was plotted against path p running along the composite-tooth (c/t) interface under loaded ridges (purple) and under loaded cusp tips (grey). (b) Von Mises stress distribution was plotted against path p running along the composite-tooth (c/t) interface for an SCR treated tooth with carious lesion (red) compared to an SCR tooth with remineralized lesion (green) and a treated tooth after NCR without carious tissue (blue).

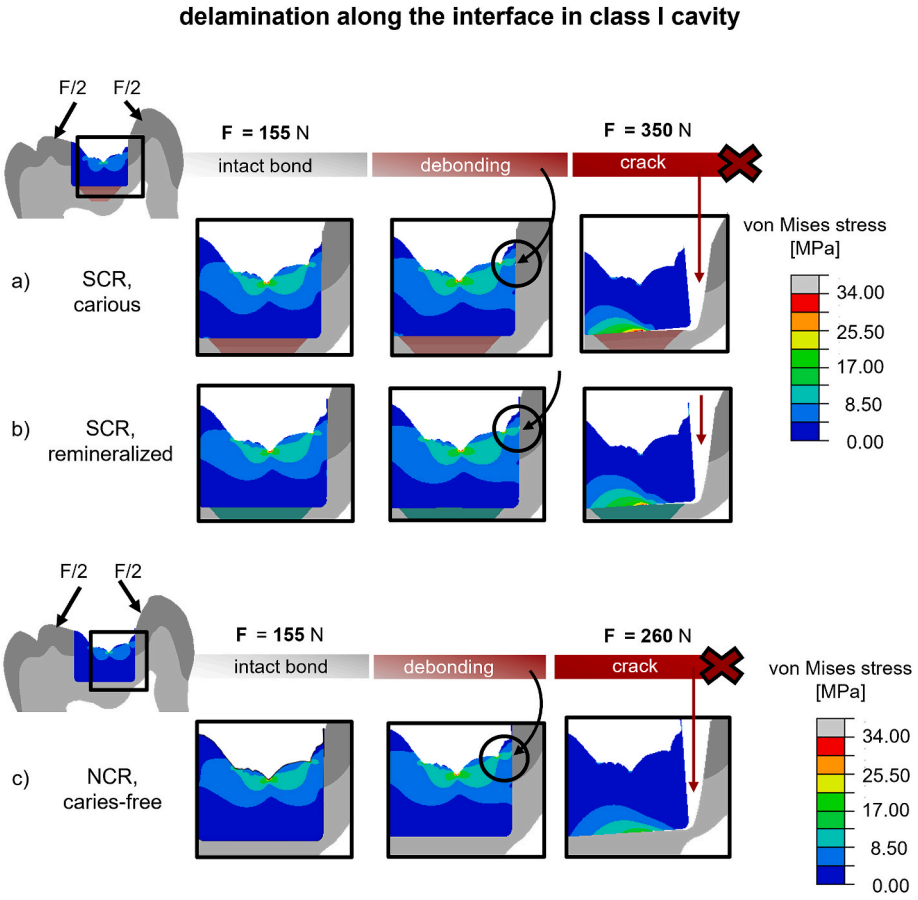

Fig. 6. Stress distribution (von Mises) was examined under loaded cusp tips in tooth with (a) class I restoration (and carious lesion beneath), (b) class I restoration (after remineralization of the carious lesion), and (c) after NCR (note: restoration cavity is larger than those after SCR).

induced peak stresses up to 13.5 MPa at the axial wall and more than twice this amount, 30 MPa, at the gingival floor (Fig. 5b). The same was observed for teeth with remineralized lesions. In NCR tooth, the interfacial stresses (4 MPa) were 43% lower than in both SCR-treated teeth with carious lesions and with remineralized lesions.

3.3. Failure of bonding - delamination along the interface in class I cavity

We studied the initiation of crack and subsequently, delamination of restoration from the tooth (also residual lesions) along the c/t interface in SCR-treated teeth with carious lesions, after remineralization and in caries-free teeth after NCR (Fig. 6). In section 3.2, the susceptibility of failure in various loading configurations was studied. In class I restoration after SCR treatment, our modeling predicted a high chance of crack at the c/t interface in all uni-axial loading models and even more pronounced in bi-axial loading on the ridges. In section 3.3, we looked into the load scenario which appeared most susceptible to failure in class I restoration after SCR treatment in the aforementioned analysis, i.e., bi-axial load at the ridges. In our dynamic model here, the sum of the initial load (F/2 + F/2) increased incrementally until the maximum local stress was achieved and thereafter, based on the assumptions of cohesive zone modeling, the cracking and delamination at the interface was initiated.

Our simulations showed that debonding initiated from the distal c/t interface of the tooth and proceeded to the pulpal regions and the proximal interfacial region. Under a summed load of 155 N, maximum von Mises stresses were found primarily at the middle part of the distal wall, initiating damage and subsequently debonding process of composite from the tooth. A visible crack, however, only appeared at a summed load of 350 N (cracking of the distal c/t interface, Fig. 6a and b) in both SCR-treated teeth with carious and remineralized lesions. Following the distal c/t interface cracking, stress levels dropped to below 5 MPa at the distal region, while a large stress concentration was then observed at the pulpal c/t interface. In case of the NCR treatment, our models predicted a visible crack only when a summed load of 260 N was reached (Fig. 6c).

4. Discussion

We present a comprehensive analysis of the biomechanical integrity of restored teeth with cavity classes I and II following treatment with selective caries removal (SCR), full caries removal (NCR), as well as post remineralization of the residual lesions. SCR is a minimally invasive treatment recommended for deeply cavitated, carious lesions. During this treatment, the caries-affected, demineralized dentin in the proximity to the pulp remains, while the rest of the carious tissue is removed from the cavitated lesion. The treated cavity is then restored with a viscous resin-based composite that, for setting, undergoes polymerization shrinkage. The biomechanical integrity of the restored SCR-treated tooth which undergoes polymerization shrinkage is neither experimentally nor numerically understood. Specifically, the role of different loading conditions acting onto the occlusal surface affecting the tooth integrity is yet to be known. In this study, finite element modeling was used to investigate the margin integrity and the longevity of the restoration-tooth interfaces post polymerization shrinkage and subjected to various loading conditions. To that aim, the spatial distribution, and magnitudes of von Mises stresses along the composite/tooth interface in class I and class II restoration were identified, and the traction-separation constitutive law was applied to predict local failure at the interface. We examined whether the softer, demineralized dentin residues weaken the mechanical integrity of the tooth-restoration complex in an SCR-treated tooth compared to NCR and to post remineralization of the lesion.

In particular, we looked into von Mises stresses induced, and failures initiated within the restoration-tooth complex after the following stages: (1) polymerization shrinkage, (2) polymerization shrinkage with subsequent several occlusal loading scenarios.

The present study complements the previous FE analyses (Weimann et al., 2021) by predicting the fracture behavior and delamination of the composite-tooth interface (modeled as a cohesive bond with the possibility of failure and cracking) which underwent composite resin polymerization shrinkage in addition to various external loading.

4.1. Residual shrinkage stress after polymerization shrinkage

Through our analysis of the polymerization shrinkage of the resin composite before loading the teeth, we found that the induced residual shrinkage stresses inside the restoration are relatively low, measuring less than 1 MPa. These results contradict the previously suggested ground truth of high residual stresses (spanning from 3 to 30 MPa) due to composite shrinkage in other studies (Ausiello et al., 2002; Bicalho et al., 2014; Dejak and Młotkowski, 2015; Soares et al., 2013). As a consequence, our analysis indicates that the actual residual stresses induced by polymerization shrinkage in the resin composite may have a smaller influence on the composite-tooth interface than initially expected for both class I and class II restorations. This suggests that other factors, such as loading conditions, cavity configurations, and material properties, might play a more significant role in determining the stress distribution and mechanical behavior of the restoration.

Previous FE studies have employed post-gel shrinkage values to compute residual shrinkage stresses after polymerization, which often overestimate the experimental values with up to orders of magnitude higher values. We have reviewed shrinkage induced stresses reported in literature and found a remarkable difference between reports of previous numerical studies to that measured in experimental settings (Fig. S1). In this study, we used the actual (i.e., experimental value) thermal coefficient (CTE) of the composite to induce more realistic and less artificially pronounced shrinkage stress inside the restoration. Doing this, we were able to compute shrinkage stress that corresponds well to experimental studies (El-Damanhoury and Platt, 2014; Keβler et al., 2019). Our data predict shrinkage stresses of less than 1 MPa that are not likely to jeopardize the integrity nor the longevity of the restoration on their own. This creates an adequate pre-stress condition, achieving long-lasting restoration in treated teeth. The notably higher shrinkage stresses shown in previous FE studies may as well be attributed to the simplifications in the simulation, such as the art of bonding between the tooth and restoration, affecting the shrinkage stress transfer and/or release. Most FE studies assume a fully bonded interface that guarantees full integrity of the restoration with an ideal stress transport through the composite-tooth assembly; however, leading to large unrealistic shrinkage stresses (Dejak and Młotkowski, 2015; Soares et al., 2013). Another common simplification is to assume the stiffness of the tooth tissues interacting with each other during polymerization, which highly impacts the resultant shrinkage stress. In our study, we took care to avoid oversimplifications by using the experimental CTE value and realistic stiffness assumptions for the tooth tissue. By incorporating these more accurate and realistic parameters, we demonstrated that the highest residual stresses, regardless of the class configuration and the dental treatment (SCR vs. NCR), are primarily concentrated at the lateral walls (i.e., mesial, distal, and axial) near the crown surface. In terms of peak stress location, our findings align with previous FE results, which also have showed interfacial peak stresses located at the coronal surface in NCR treated molars (Da Silva Pereira et al., 2020; Kowalczy and Gambin, 2008). This consistency in peak stress location further sports the validity and reliability of our current study's predictions.

Regardless of the class configuration, this study indicates that non-uniform stresses occur at the composite/tooth interface due to polymerization kinetics. The presence of adhesion between composite and tooth (i.e., bonded surfaces) hinders the polymerization shrinkage at the cavity walls, resulting in a gradual decrease in deformation (strain) and consequently the induced stresses. This means that the stresses at the c/t interface are not evenly distributed, and the adhesion between the materials plays a significant role in managing these stresses during

polymerization. The composite portion neighboring the free occlusal surface (unbonded surface), in contrast, polymerizes non-restrictively, which enables an inward displacement of the composite towards the pulp. As a result, the composite material can undergo inward displacements towards the pulp, potentially explaining why higher shrinkage stress levels are detected at the coronal surface compared to the bottom of the cavity. Importantly, shrinkage stresses induced in SCR-treated teeth were predicted to be similar to that of the NCR treated. This suggests that the presence of carious tissue does not affect the shrinkage behavior of the composite during polymerization nor the resultant shrinkage stress along the c/t interface.

This study also reveals an interesting observation within the restoration material, where a decrease in shrinkage stress was observed from the c/t interface towards the core of the restoration material. Specifically, this decrease in shrinkage stress is found to be significant, reaching up to 50% reduction in both class I and class II cavities (Fig. 3). The internal stress reduction within the restoration material is noteworthy, as it indicates a potential stress-relieving effect within the bulk of the resin composite. As the polymerization reaction progresses from the c/t interface into the restoration, the stresses generated may be partially dissipated or compensated for due to factors like material flow, resin flow, and cavity adaptation. This is a typical shrinkage behavior for a solid bulk material, while untypical for an inhomogeneous (e.g., layered material) (Bicalho et al., 2014). It is well-known that the filling technique induces different stress patterns within the restoration (Bicalho et al., 2014; Oliveira et al., 2013). Bulk fill resin composites strongly react to light polymerization, which improves the depth of cure. This enables the placement of the composite in one single step producing one continuous interface between composite and interface, instead of several small interfaces inserted by the incremental technique. The bulk fill technique, thus, simplifies the filling procedure and shortens the application time compared to conventional composites (Da Silva Pereira et al., 2020; Duarte et al., 2020; Kim et al., 2015; Loguercio et al., 2019; Park et al., 2021; Sampaio et al., 2017; Yazici et al., 2017). The incremental filling technique, in contrast, is said to reduce the shrinkage stress at the tooth composite interface by permitting the stress-relieving flow of the composite from the unbounded surface toward the bonded surface (Feilzer et al., 1987; Kim et al., 2015; Kwon et al., 2012; Rosatto et al., 2015; Soares et al., 2013).

Importantly, shrinkage stresses induced in SCR-treated teeth were predicted to be similar to that of the NCR treated. This suggests that the presence of carious tissue does not affect the shrinkage behavior of the composite during polymerization nor the resultant shrinkage stress along the c/t interface. Another important aspect notable to consider in the context of polymerization shrinkage are the advancement in light-curing resin composites and the modern bulk-filling resin composites, which have different chemistry and shrinkage characteristics compared to traditional ones (van Ende et al., 2017). The amount of shrinkage stress depends on factors, such as curing light intensity, photo-activation time, mechanical properties of tooth structure (Apicella et al., 2002; Chuang et al., 2016; Kwon et al., 2012; Rosatto et al., 2015; Topa-Skwarczyńska and Ortyl, 2023). Although these aspects are not covered within the context of the current study, it sheds light on the broader implications and provides guidance for future investigations in this area.

4.2. Stress response to various occlusal loading in addition to residual shrinkage stresses

We conducted a thorough examination of the load response of the SCR-restored teeth with resin in both class I and class II cavities after polymerization shrinkage. As anticipated, the finding revealed substantial differences in stress distribution between two cavity classes, depending on the treatment and the loading conditions applied. The location and magnitude of peak stresses in SCR-treated teeth were significantly influenced by the specific loading scenario.

In **class I restorations**, we found high von Mises stresses (>17 MPa) along the mesial wall under bi-axial loading, while under uni-axial loading, lower peak stresses (<12.75 MPa) were found along the pulpal floor of the restoration. Both loading scenarios, under a physiologic masticatory load of 100 N, have the potential to compromise and lead to failure of the restoration. As hypothesized, the predicted stress distribution for class I restorations with remineralized lesions and after complete caries removal (NCR) was substantially different from those with SCR-treated teeth. We demonstrated that the presence of carious lesions substantially affects the stress distributions and magnitudes. Carious lesions are characterized by soft demineralized tissue with low stiffness. Compared to the other hard tissues, such as enamel, dentin and resin composite, carious lesions have the lowest mineral content within the tooth structure. Consequently, their reduced mechanical properties may contribute to stress absorption and reduction. Interestingly, our analysis revealed that complete caries removal and remineralization of the SCR-treated teeth could still result in restoration compromise. However, the compromised areas were observed at anatomical locations more distal to the tooth.

In **class II restoration**, we found that bi-axial loading scenarios do not pose a threat to the tooth-restoration integrity. Our investigation of stresses induced under two bi-axial loading scenarios (ridges and cusp tips) showed lower stress values than the bond strength, indicating that the mechanical integrity of the c/t interface is not compromised under these loading conditions. Under uni-axial loading, however, stresses exceeded the bond strength of 8.56 MPa at both axial and gingival regions, suggesting a compromised mechanical integrity of the interface. This observation was consistent in the teeth with remineralized lesion as well. A noteworthy finding was that, regardless of the caries treatment, our simulations revealed high stress peaks at the gingival margin under uni-axial loading with an increased the risk of failure. This indicates that the gingival margin is a critical area that is particularly vulnerable to potential restoration failure, in class II restorations. Similar results have been detected in studies showing that the gingival margin in class II composite restorations is the most common location of bonding failures (Duarte et al., 2020; Spencer et al., 2010).

4.3. Failure of bonding in class I cavity

We then focused on investigating the initiation of cracks and subsequent delamination of the restoration from the tooth, including residual lesions, along the c/t interface. For Class I restorations after SCR treatment, our static modeling predicted high stresses and consequently a high likelihood of cracks at the c/t interface in all uni-axial loading models, and this susceptibility was even more pronounced under bi-axial loading on the ridges. Therefore, here we focused on the load scenario that appeared most susceptible to failure in Class I restorations after SCR treatment, specifically, the bi-axial load at the ridges. The crack initiation and propagation were investigated using an advanced dynamic FE model, in which we incrementally increased the sum of the initial load until the initiation of cracking and delamination at the c/t interface occurred and progressed.

The simulations revealed that debonding initiated from the distal c/t interface of the tooth and progressed towards the pulpal regions and the proximal interfacial region. Under a summed load of 155 N, maximum von Mises stresses were primarily observed at the middle part of the distal wall, leading to damage initiation and subsequent debonding of the composite from the tooth. However, a visible crack appeared only at a summed load of 350 N in both SCR-treated teeth with carious and remineralized lesions. Following the cracking of the distal c/t interface, stress levels decreased to below 5 MPa at the distal region, while a large stress concentration was observed at the pulpal c/t interface. In contrast, for NCR-treated teeth, our models predicted a visible crack much earlier, when already a summed load of 260 N was reached.

These findings offer valuable insights into the mechanical behavior of SCR-treated teeth under different loading conditions and underscore the significance of considering the specific load scenarios that may lead

to failure at the composite-tooth interface. It is important to note that the tooth models assume the filling material to be homogeneous. In clinical situations, inhomogeneities such as voids (Sampaio et al., 2017), air bubble entrapment, and contaminants may happen within resin composite filling (Belnoue et al., 2016) affecting crack initiation and propagation. Nevertheless, the results clearly demonstrate the biomechanical advantages of SCR treatment in preserving the integrity of the tooth/restoration complex. By understanding the factors influencing crack initiation and delamination, this in silico study is the first of its kind that contributes to the optimization of restorative treatments and aids in the design of more resilient dental restorations.

5. Conclusions

This finite element study aimed to assess the stress distribution in teeth restored with selective caries removal (SCR) and restored with resin composite in class I and class II cavities, as well as in SCR-treated teeth with remineralized lesions and caries-free teeth restored after complete caries removal (NCR). Despite certain limitations, the study draws the following conclusions:

(1) Residual shrinkage stress: The study observed that residual shrinkage stress was generated at the bonded interface during polymerization shrinkage of the resin composite, highlighting the importance of considering and managing the effect of polymerization shrinkage on the tooth-restoration complex.
(2) Tolerability of polymerization shrinkage stresses: The polymerization shrinkage stresses were found to be bearable for the treated teeth, regardless of the class type (class I or class II).
(3) Increased risk of debonding: Under cusp tips loading conditions, SCR-treated teeth with class I restorations exhibited an increased risk of debonding along the vertical cavity walls, indicating the potentially compromised load-bearing capacity of class I restorations in SCR -treated teeth under specific occlusal loading conditions. (4) Margin integrities: Our study rejected the null hypothesis by demonstrating that teeth treated with selective caries removal (SCR) exhibited superior marginal integrities compared to teeth restored after complete caries removal (NCR). These findings contribute to the understanding of the biomechanics of dental restorations and support evidence-based decision-making in restorative dentistry. Further research and clinical validation are necessary to strengthen and expand upon these conclusions.

CRediT authorship contribution statement

Dominique Weimann: Writing – review & editing, Writing – original draft, Visualization, Validation, Methodology, Investigation, Formal analysis, Data curation, Conceptualization. **Claudia Fleck:** Writing – review & editing, Supervision, Funding acquisition, Conceptualization. **Hajar Razi:** Writing – review & editing, Validation, Supervision, Methodology, Investigation, Formal analysis, Data curation, Conceptualization.

Declaration of competing interest

The authors declare that they have no known competing financial interests or personal relationships that could have appeared to influence the work reported in this paper.

Data availability

Data will be made available on request.

Acknowledgements

We gratefully acknowledge the North German Supercomputing Alliance (HLRN) for the use of their computing resources and Dr.-Ing. Baumann for his invaluable advice.

Appendix A. Supplementary data

Supplementary data to this article can be found online at https://doi.org/10.1016/j.jmbbm.2024.106554.

References

Alnazzawi, A., Watts, D.C., 2012. Simultaneous determination of polymerization shrinkage, exotherm and thermal expansion coefficient for dental resin-composites. Dent. Mater. : Off. Publ. Acad. Dent. Mater. 28 (12), 1240–1249. https://doi.org/10.1016/j.dental.2012.09.004.

Alves, L.S., Fontanella, V., Damo, A.C., Ferreira de Oliveira, E., Maltz, M., 2010. Qualitative and quantitative radiographic assessment of sealed carious dentin: a 10-year prospective study. Oral Surg. Oral Med. Oral Pathol. Oral Radiol. Endod. 109 (1), 135–141. https://doi.org/10.1016/j.tripleo.2009.08.021.

Apicella, A., Palma, L., Aversa, R., 2002. DSC kinetic characterization of dental composites using different light sources. J. Adv. Mater. 22–25.

Ausiello, P., Apicella, A., Davidson, C., 2002. Effect of adhesive layer properties on stress distribution in composite restorations - a 3D finite element analysis. Dent. Mater. (18), 295–303.

Ausiello, P., Ciaramella, S., Martorelli, M., Lanzotti, A., Gloria, A., Watts, D.C., 2017. CAD-FE modeling and analysis of class II restorations incorporating resin-composite, glass ionomer and glass ceramic materials. Dent. Mater. : Off. Publ. Acad. Dent. Mater. 33 (12), 1456–1465. https://doi.org/10.1016/j.dental.2017.10.010.

Bedon, C., Machalická, K., Eliášová, M., Vokáč, M., 2018. Numerical modelling of adhesive connections including cohesive damage. In: 309-320 Pages/Challenging Glass Conference Proceedings, vol. 6. https://doi.org/10.7480/CGC.6.2155 (2018): Challenging Glass 6.

Belnoue, J.P.-H., Giannis, S., Dawson, M., Hallett, S.R., 2016. Cohesive/adhesive failure interaction in ductile adhesive joints Part II: quasi-static and fatigue analysis of double lap-joint specimens subjected to through-thickness compressive loading. Int. J. Adhesion Adhes. 68, 369–378. https://doi.org/10.1016/j.ijadhadh.2016.03.010.

Betancourt, D.E., Baldion, P.A., Castellanos, J.E., 2019. Resin-dentin bonding interface: mechanisms of degradation and strategies for stabilization of the hybrid layer. Int. J. Biomater. 2019, 5268342 https://doi.org/10.1155/2019/5268342.

Bicalho, A.A., Valdívia, A.D.C.M., Barreto, B.C.F., Tantbirojn, D., Versluis, A., Soares, C. J., 2014. Incremental filling technique and composite material–part II: shrinkage and shrinkage stresses. Operat. Dent. 39 (2), E83–E92. https://doi.org/10.2341/12-442-L.

Boaro, L.C.C., Gonçalves, F., Guimarães, T.C., Ferracane, J.L., Versluis, A., Braga, R.R., 2010. Polymerization stress, shrinkage and elastic modulus of current low-shrinkage restorative composites. Dent. Mater. : Off. Publ. Acad. Dent. Mater. 26 (12), 1144–1150. https://doi.org/10.1016/j.dental.2010.08.003.

Braga, R.R., Boaro, L.C.C., Kuroe, T., Azevedo, C.L.N., Singer, J.M., 2006. Influence of cavity dimensions and their derivatives (volume and 'C' factor) on shrinkage stress development and microleakage of composite restorations. Dent. Mater. : Off. Publ. Acad. Dent. Mater. 22 (9), 818–823. https://doi.org/10.1016/j.dental.2005.11.010.

Cakir, D., Sergent, R., Burgess, J.O., 2007. Clinical materials review: polymerization shrinkage - clinical review. Inside Dent. https://www.aegisdentalnetwork.com/id/2007/09/polymerization-shrinkage-clinical-review.

Chen, T.Y.-F., Huang, P.-S., Chuang, S.-F., 2014. Modeling dental composite shrinkage by digital image correlation and finite element methods. Opt Laser. Eng. 61, 23–30. https://doi.org/10.1016/j.optlaseng.2014.04.006.

Chiang, M.Y.M., Giuseppetti, A.A.M., Qian, J., Dunkers, J.P., Antonucci, J.M., Schumacher, G.E., Gibson, S.-L., 2011. Analyses of a cantilever-beam based instrument for evaluating the development of polymerization stresses. Dent. Mater. : Off. Publ. Acad. Dent. Mater. 27 (9), 899–905. https://doi.org/10.1016/j.dental.2011.05.006.

Chuang, S.-F., Chang, C.-H., Chen, T.Y.-F., 2011. Contraction behaviors of dental composite restorations–finite element investigation with DIC validation. J. Mech. Behav. Biomed. Mater. 4 (8), 2138–2149. https://doi.org/10.1016/j.jmbbm.2011.07.014.

Chuang, S.-F., Huang, P.-S., Chen, T.Y.-F., Huang, L.-H., Su, K.-C., Chang, C.-H., 2016. Shrinkage behaviors of dental composite restorations-The experimental-numerical hybrid analysis. Dent. Mater. : Off. Publ. Acad. Dent. Mater. 32 (12), e362–e373. https://doi.org/10.1016/j.dental.2016.09.022.

Correia, A.M., Tribst, J., Matos, F.d.S., Platt, J.A., Caneppele, T.M.F., Borges, A.L.S., 2018. Polymerization shrinkage stresses in different restorative techniques for non-carious cervical lesions. J. Dent. 76, 68–74. https://doi.org/10.1016/j.jdent.2018.06.010.

Da Silva Pereira, R.A., Bragança, G.F. de, Vilela, A., Deus, R.A. de, Miranda, R.R., Veríssimo, C., Soares, C.J., 2020. Post-gel and total shrinkage stress of conventional and bulk-fill resin composites in endodontically-treated molars. Operat. Dent. 45 (5), E217–E226. https://doi.org/10.2341/19-187-L.

Davidson, C.L., Feilzer, A.J., 1997. Polymerization shrinkage and polymerization shrinkage stress in polymer-based restoratives. J. Dent. 25 (6), 435–440.

Dejak, B., Młotkowski, A., 2015. A comparison of stresses in molar teeth restored with inlays and direct restorations, including polymerization shrinkage of composite resin and tooth loading during mastication. Dent. Mater. : Off. Publ. Acad. Dent. Mater. 31 (3), e77–e87. https://doi.org/10.1016/j.dental.2014.11.016.

Di Lauro, A., Di Duca, F., Montuori, P., Dal Piva, A.M.d.O., Tribst, J.P.M., Borges, A.L.S., Ausiello, P., 2023. Fluoride and calcium release from alkasite and glass ionomer restorative dental materials: in vitro study. J. Funct. Biomater. 14 (2) https://doi.org/10.3390/jfb14020109.

Diehl, T., 2008. On using a penalty-based cohesive-zone finite element approach, Part I: elastic solution benchmarks. Int. J. Adhesion Adhes. 28 (4–5), 237–255. https://doi.org/10.1016/j.ijadhadh.2007.06.003.

Duarte, J.C.L., Costa, A.R., Veríssimo, C., Duarte, R.W., Calabrez Filho, S., Spohr, A.M., Borges, G.A., Correr-Sobrinho, L., 2020. Interfacial stress and bond strength of bulk-fill or conventional composite resins to dentin in class II restorations. Braz. Dent. J. 31 (5), 532–539. https://doi.org/10.1590/0103-6440202003338.

El-Damanhoury, H., Platt, J., 2014. Polymerization shrinkage stress kinetics and related properties of bulk-fill resin composites. Operat. Dent. 39 (4), 374–382. https://doi.org/10.2341/13-017-L.

Elgezawi, M., Haridy, R., Abdalla, M.A., Heck, K., Draenert, M., Kaisarly, D., 2022. Current strategies to control recurrent and residual caries with resin composite restorations: operator- and material-related factors. J. Clin. Med. 11 (21) https://doi.org/10.3390/jcm11216591.

Feilzer, A.J., Gee, A.J. de, Davidson, C.L., 1987. Setting stress in composite resin in relation to configuration of the restoration. J. Dent. Res. 66 (11), 1636–1639. https://doi.org/10.1177/00220345870660110601.

Franzon, R., Opdam, N.J., Guimarães, L.F., Demarco, F.F., Casagrande, L., Haas, A.N., Araujo, F.B., 2015. Randomized controlled clinical trial of the 24-months survival of composite resin restorations after one-step incomplete and complete excavation on primary teeth. J. Dent. 43 (10), 1235–1241. https://doi.org/10.1016/j.jdent.2015.07.011.

Fronza, B.M., Rueggeberg, F.A., Braga, R.R., Mogilevych, B., Soares, L.E.S., Martin, A.A., Ambrosano, G., Giannini, M., 2015. Monomer conversion, microhardness, internal marginal adaptation, and shrinkage stress of bulk-fill resin composites. Dent. Mater. : Off. Publ. Acad. Dent. Mater. 31 (12), 1542–1551. https://doi.org/10.1016/j.dental.2015.10.001.

Gilabert, F.A., Garoz, D., van Paepegem, W., 2015. Stress concentrations and bonding strength in encapsulation-based self-healing materials. Mater. Des. 67, 28–41. https://doi.org/10.1016/j.matdes.2014.11.012.

Gözetici-Çil, B., Erdem-Hepşenoğlu, Y., Tekin, A., Özcan, M., 2023. Selective removal to soft dentine or selective removal to firm dentine for deep caries lesions ın permanent posterior teeth: a randomized controlled clinical trial up to 2 years. Clin. Oral Invest. 27 (5), 2125–2137. https://doi.org/10.1007/s00784-022-04815-0.

Haddad, M., Sepehrnoori, K., 2015. Simulation of hydraulic fracturing in quasi-brittle shale formations using characterized cohesive layer: stimulation controlling factors. J. Unconvent. Oil Gas Resour. 9, 65–83. https://doi.org/10.1016/j.juogr.2014.10.001.

Harper, P.W., Hallett, S.R., 2010. A fatigue degradation law for cohesive interface elements – development and application to composite materials. Int. J. Fatig. 32 (11), 1774–1787. https://doi.org/10.1016/j.ijfatigue.2010.04.006.

Hickmann, J., Jacobsen, P.H., 1991. Finite element analysis of dental polymeric. Clin. Mater. 7, 39–43.

Hirata, R., Clozza, E., Giannini, M., Farrokhmanesh, E., Janal, M., Tovar, N., Bonfante, E. A., Coelho, P.G., 2015. Shrinkage assessment of low shrinkage composites using micro-computed tomography. J. Biomed. Mater. Res. B Appl. Biomater. 103 (4), 798–806. https://doi.org/10.1002/jbm.b.33258.

Ikramullah, Afrizal, A., Huzni, S., Thalib, S., Abdul Khalil, H.P.S., Rizal, S., 2020. Effect of mesh sensitivity and cohesive properties on simulation of Typha fiber/epoxy microbond test. Computation 8 (1), 2. https://doi.org/10.3390/computation8010002.

Ilie, N., Hickel, R., 2011. Investigations on a methacrylate-based flowable composite based on the SDR™ technology. Dent. Mater. : Off. Publ. Acad. Dent. Mater. 27 (4), 348–355. https://doi.org/10.1016/j.dental.2010.11.014.

Jardim, J.J., Mestrinho, H.D., Koppe, B., Paula, L.M. de, Alves, L.S., Yamaguti, P.M., Almeida, J.C.F., Maltz, M., 2020. Restorations after selective caries removal: 5-Year randomized trial. J. Dent. 99, 103416 https://doi.org/10.1016/j.jdent.2020.103416.

Jousset, P., Rachik, M., 2014. Comparison and evaluation of two types of cohesive zone models for the finite element analysis of fracture propagation in industrial bonded structures. Eng. Fract. Mech. 132, 48–69. https://doi.org/10.1016/j.engfracmech.2014.10.018.

Keßler, A., Kaisarly, D., Hickel, R., Kunzelmann, K.-H., 2019. Effect of fiber incorporation on the contraction stress of composite materials. Clin. Oral Invest. 23 (3), 1461–1471. https://doi.org/10.1007/s00784-018-2572-1.

Kim, R.J.-Y., Kim, Y.-J., Choi, N.-S., Lee, I.-B., 2015. Polymerization shrinkage, modulus, and shrinkage stress related to tooth-restoration interfacial debonding in bulk-fill composites. J. Dent. 43 (4), 430–439. https://doi.org/10.1016/j.jdent.2015.02.002.

Kleverlaan, C.J., Feilzer, A.J., 2005. Polymerization shrinkage and contraction stress of dental resin composites. Dent. Mater. : Off. Publ. Acad. Dent. Mater. 21 (12), 1150–1157. https://doi.org/10.1016/j.dental.2005.02.004.

Kowalczy, P., Gambin, W., 2008. Techniques of shrinkage stress reduction in dental restorations. Int. J. Material Form. 1 (S1), 755–758. https://doi.org/10.1007/s12289-008-0285-8.

Kwon, Y., Ferracane, J., Lee, I.-B., 2012. Effect of layering methods, composite type, and flowable liner on the polymerization shrinkage stress of light cured composites. Dent. Mater. : Off. Publ. Acad. Dent. Mater. 28 (7), 801–809. https://doi.org/10.1016/j.dental.2012.04.028.

Laughlin, G.A., Williams, J., Eick, J., 2002. The influence of system compliance and sample geometry on composite polymerization shrinkage stress. J. Biomed. Mater. Res. 63 (5), 671–678.

Li, H., Li, J., Zou, Z., Fok, A.S.-L., 2011. Fracture simulation of restored teeth using a continuum damage mechanics failure model. Dent. Mater. : Off. Publ. Acad. Dent. Mater. 27 (7), e125–e133. https://doi.org/10.1016/j.dental.2011.03.006.

Li, J., Thakur, P., Fok, A.S.L., 2014. Shrinkage of dental composite in simulated cavity measured with digital image correlation. J. Vis. Exp. 89 https://doi.org/10.3791/51191.

Lim, Z.E., Duncan, H.F., Moorthy, A., McReynolds, D., 2023. Minimally invasive selective caries removal: a clinical guide. Br. Dent. J. 234 (4), 233–240. https://doi.org/10.1038/s41415-023-5515-4.

Lins, R., Vinagre, A., Alberto, N., Domingues, M.F., Messias, A., Martins, L.R., Nogueira, R., Ramos, J.C., 2019a. Polymerization shrinkage evaluation of restorative resin-based composites using fiber bragg grating sensors. Polymers 11 (5). https://doi.org/10.3390/polym11050859.

Lins, R.B.E., Aristilde, S., Osório, J.H., Cordeiro, C.M.B., Yanikian, C.R.F., Bicalho, A.A., Stape, T.H.S., Soares, C.J., Martins, L.R.M., 2019b. Biomechanical behaviour of bulk-fill resin composites in class II restorations. J. Mech. Behav. Biomed. Mater. 98, 255–261. https://doi.org/10.1016/j.jmbbm.2019.06.032.

Loguercio, A.D., Rezende, M., Gutierrez, M.F., Costa, T.F., Armas-Vega, A., Reis, A., 2019. Randomized 36-month follow-up of posterior bulk-filled resin composite restorations. J. Dent. 85, 93–102. https://doi.org/10.1016/j.jdent.2019.05.018.

Lundgren, D., Laurell, L., 1986. Occlusal force pattern during chewing and biting in dentitions restored with fixed bridges of cross-arch extension. J. Oral Rehabil. (13), 57–71. https://doi.org/10.1111/j.1365-2842.1986.tb01556.x.

Maltz, M., Jardim, J.J., Mestrinho, H.D., Yamaguti, P.M., Podestá, K., Moura, M.S., Paula, L.M. de, 2013. Partial removal of carious dentine: a multicenter randomized controlled trial and 18-month follow-up results. Caries Res. 47 (2), 103–109. https://doi.org/10.1159/000344013.

Mantri, S.P., Mantri, S.S., 2013. Management of shrinkage stresses in direct restorative light-cured composites: a review. J. Esthetic Restor. Dent. : Off. Publ. Am. Acad. Esthet. Dent. [et al.] 25 (5), 305–313. https://doi.org/10.1111/jerd.12047.

Moga, R.A., Olteanu, C.D., Daniel, B.M., Buru, S.M., 2023. Finite elements analysis of tooth-A comparative analysis of multiple failure criteria. Int. J. Environ. Res. Publ. Health 20 (5). https://doi.org/10.3390/ijerph20054133.

Nascimento, A.S., Rodrigues, J.F.B., Torres, R.H.N., Santos, K.O., Fook, M.V.L., Albuquerque, M.S. de, Lima, E.A. de, Filgueira, P.T.D., Santos, J.B.M.D., Oliveira, L. J.R. de, Braz, R., 2019. Physicomechanical and thermal analysis of bulk-fill and conventional composites. Braz. Oral Res. 33, e008 https://doi.org/10.1590/1807-3107bor-2019.vol33.0008.

Oliveira, K.M.C., Lancellotti, A.C.R.A., Ccahuana-Vásquez, R.A., Consani, S., 2013. Influence of filling techniques on shrinkage stress in dental composite restorations. J. Dent. Sci. 8 (1), 53–60. https://doi.org/10.1016/j.jds.2012.01.015.

Paneda, E.M., 2018. Abaqus Implementation of Cohesive Zone Models, pp. 1–20.

Park, K.-J., Pfeffer, M., Näke, T., Schneider, H., Ziebolz, D., Haak, R., 2021. Evaluation of low-viscosity bulk-fill composites regarding marginal and internal adaptation. Odontology 109 (1), 139–148. https://doi.org/10.1007/s10266-020-00531-x.

Peutzfeldt, A., 1997. Resin composites in dentistry: the monomer systems. Eur. J. Oral Sci. 105, 97–116.

Pugach, M.K., Strother, J., Darling, C.L., Fried, D., Gansky, S.A., Marshall, S.J., Marshall, G.W., 2009. Dentin caries zones: mineral, structure, and properties. J. Dent. Res. 88 (1), 71–76. https://doi.org/10.1177/0022034508327552.

Rajan, G., Raju, R., Jinachandran, S., Farrar, P., Xi, J., Prusty, B.G., 2019. Polymerisation shrinkage profiling of dental composites using optical fibre sensing and their correlation with degree of conversion and curing rate. Sci. Rep. 9 (1), 3162. https://doi.org/10.1038/s41598-019-40162-z.

Robinson, D., Aguilar, L., Gatti, A., Abduo, J., Lee, P.V.S., Ackland, D., 2019. Load response of the natural tooth and dental implant: a comparative biomechanics study. J. Adv. Prosthodont. 11 (3), 169–178. https://doi.org/10.4047/jap.2019.11.3.169.

Rosatto, C.M.P., Bicalho, A.A., Veríssimo, C., Bragança, G.F., Rodrigues, M.P., Tantbirojn, D., Versluis, A., Soares, C.J., 2015. Mechanical properties, shrinkage stress, cuspal strain and fracture resistance of molars restored with bulk-fill composites and incremental filling technique. J. Dent. 43 (12), 1519–1528. https://doi.org/10.1016/j.jdent.2015.09.007.

Sakaguchi, R.L., Wiltbank, B.D., Shah, N.C., 2004. Critical configuration analysis of four methods for measuring polymerization shrinkage strain of composites. Dent. Mater. : Off. Publ. Acad. Dent. Mater. 20 (4), 388–396. https://doi.org/10.1016/j.dental.2003.11.002.

Sampaio, C.S., Chiu, K.-J., Farrokhmanesh, E., Janal, M., Puppin-Rontani, R.M., Giannini, M., Bonfante, E.A., Coelho, P.G., Hirata, R., 2017. Microcomputed tomography evaluation of polymerization shrinkage of class I flowable resin composite restorations. Operat. Dent. 42 (1), E16–E23. https://doi.org/10.2341/15-296-L.

Schwendicke, F., Splieth, C., Breschi, L., Banerjee, A., Fontana, M., Paris, S., Burrow, M. F., Crombie, F., Page, L.F., Gatón-Hernández, P., Giacaman, R., Gugnani, N., Hickel, R., Jordan, R.A., Leal, S., Lo, E., Tassery, H., Thomson, W.M., Manton, D.J., 2019. When to intervene in the caries process? An expert Delphi consensus statement. Clin. Oral Invest. 23 (10), 3691–3703. https://doi.org/10.1007/s00784-019-03058-w.

Shao, J.R., Liu, N., Zheng, Z.J., 2022. A modified progressive damage model for simulating low-velocity impact of composite laminates. Adv. Mech. Eng. 14 (5), 168781322210959 https://doi.org/10.1177/16878132221095948.

Soares, C.J., Bicalho, A.A., Tantbirojn, D., Versluis, A., 2013. Polymerization shrinkage stresses in a premolar restored with different composite resins and different

incremental techniques. J. Adhesive Dent. 15 (4), 341–350. https://doi.org/10.3290/j.jad.a29012.

Soares, C.J., Faria-E-Silva, A.L., Rodrigues, M.d.P., Vilela, A.B.F., Pfeifer, C.S., Tantbirojn, D., Versluis, A., 2017. Polymerization shrinkage stress of composite resins and resin cements - what do we need to know? Braz. Oral Res. 31 (Suppl. 1), e62 https://doi.org/10.1590/1807-3107BOR-2017.vol31.0062.

Spencer, P., Ye, Q., Park, J., Topp, E.M., Misra, A., Marangos, O., Wang, Y., Bohaty, B.S., Singh, V., Sene, F., Eslick, J., Camarda, K., Katz, J.L., 2010. Adhesive/Dentin interface: the weak link in the composite restoration. Ann. Biomed. Eng. 38 (6), 1989–2003. https://doi.org/10.1007/s10439-010-9969-6.

Tjäderhane, L., Tezvergil-Mutluay, A., 2019. Performance of adhesives and restorative materials after selective removal of carious lesions: restorative materials with anticaries properties. Dent. Clin. 63 (4), 715–729. https://doi.org/10.1016/j.cden.2019.05.001.

Topa-Skwarczyńska, M., Ortyl, J., 2023. Photopolymerization shrinkage: strategies for reduction, measurement methods and future insights. Polym. Chem. 14 (18), 2145–2158. https://doi.org/10.1039/D3PY00261F.

van Ende, A., Munck, J. de, Lise, D.P., van Meerbeek, B., 2017. Bulk-fill composites: a review of the current literature. J. Adhesive Dent. 19 (2), 95–109. https://doi.org/10.3290/j.jad.a38141.

Versluis, A., Tantbirojn, D., Pintado, M.R., DeLong, R., Douglas, W.H., 2004. Residual shrinkage stress distributions in molars after composite restoration. Dent. Mater. : Off. Publ. Acad. Dent. Mater. 20 (6), 554–564. https://doi.org/10.1016/j.dental.2003.05.007.

Wang, Y., Woodworth, L., Han, B., 2011. Simultaneous measurement of effective chemical shrinkage and modulus evolutions during polymerization. Exp. Mech. 51 (7), 1155–1169. https://doi.org/10.1007/s11340-010-9410-y.

Weimann, D., Morgenthal, A., Schwendicke, F., Fleck, C., Razi, H., 2021. Substantial regional differences in the biomechanical behavior of molar treated with selective caries tissue removal technique: a finite element study. Dent. Mater. : Off. Publ. Acad. Dent. Mater. 37 (3), e162–e175. https://doi.org/10.1016/j.dental.2020.11.008.

Widbiller, M., Weiler, R., Knüttel, H., Galler, K.M., Buchalla, W., Scholz, K.J., 2022. Biology of selective caries removal: a systematic scoping review protocol. BMJ Open 12 (2), e061119. https://doi.org/10.1136/bmjopen-2022-061119.

Yazici, A.R., Antonson, S.A., Kutuk, Z.B., Ergin, E., 2017. Thirty-six-Month clinical comparison of bulk fill and nanofill composite restorations. Operat. Dent. 42 (5), 478–485. https://doi.org/10.2341/16-220-C.